Time-Frequency Investigation of Heart Rate Variability and Respiratory Signal Using Adaptive Continuous Morlet Wavelet Transform

Ram Sewak Singh[a]*, R.P.S. Chauhan [b], Demissie Jobir Gelmecha[a], Tadesse Hailu [a], Praveen Kumar [b] and Lakhan Dev Sharma[c]

[a]*Electronics & Communication Eng. Department*
School of Electrical Engineering & Computing
Adama Science & Technology University, Ethiopia, Adama.
[b] *Department of Electronics and Communication Engineering,*
IMS Engineering College, Ghaziabad, Uttar Pradesh, India.
[c]*Department of Electronics and Communication Engineering,*
MLV Textile and Engineering College, Bhilwara, Rajasthan, India
*ramsewaknitj@gmail.com

Received: *07.11.2019,* ***Accepted:*** *16.03.2020*

ABSTRACT

Precise spectral assessment of heart rate variability (HRV) and respiratory signal provides valuable information for clinical setting and diagnoses any cardiac abnormalities as well as detection of cardiac disease. The wavelet transform (WT) methods have emerged over recent years as an influential tool to interrogate of non-stationary HRV and respiratory signals in frequency and time-frequency domain. The emerging function of an adaptive continuous Morlet wavelet transformation (ACMWT) method was used in this paper to analysis HRV's time-frequency physiognomies and respiratory signals of healthy young (HYNG) and elderly (HELY) subjects. Adaptation of this technique was based on maximum energy concentration. First, ACMWT has been validated on non-stationary artificial signals as similar to dynamic changes in HRV signals. A goodness of fit test as Kolmogorov-Smirnov (KS) test and autocorrelation function (AFC) in the form of transformed quantiles was also used to test the robustness of proposed method. ACMWT was observed to be comparatively better within the desired confidence limits. The power spectral characteristics of HRV signals of HYNG and HELY subjects were demonstrated in time-frequency domain and measured the value using median interquartile range of band power spectra. Global results show that HRV's low-frequency power spectra (LFp) and high-frequency power spectra (HFp) indices are decreased in HEG relative to HYG subjects ($p<0.0001$).

Keywords - Adaptive Morlet wavelet method, Maximum energy concentration, Power spectral methods, Heart Rate Variability, Respiratory.

1. INTRODUCTION

Generally, variations of cardiovascular signals, especially the heart rate variability (HRV) and respiratory signals are investigated in the time domain by expert physicians. But diseases related to cardiac may not generally be evident in the time-domain analysis (Bigan and Woolfson, 2000). This conventional strategy for diagnosis seen that the accuracy and the precision of the diagnosis relies upon the expertise cardiologist. However, time domain provides the excellent time resolution, but does not give spectral information. The sympathetic and parasympathetic activity of autonomic nerves system (ANS), breathing, thermoregulatory cycles (R I KITNE, 1980) or fluctuations related to plasma renin activity (Koh *et al.,* 1994; D. L. Eckberg, 1985), including changes of activity, posture, autonomic outflow, temperature regulation, state of arousal (CJ *et al.,* 2001; Vornanen, Ryökkynen and Nurmi, 2002), humoral system, efferent neural information from arterial baroreceptors to the cardio regulatory center, myocardial contractility and systemic vascular resistance are functioning or visible in particular frequency band (Kamath et al., 1987; Kamath and Fallen, 1993). This reality has persuaded the utilization of frequency domain strategies, for example, Fourier transform (FT), for investigation

(Clayton and Murray, 1993). As FT is a result of integration between infinite time duration, hence analysis is averaged of HRV and respiratory time series signal. Thus, this method only provides globally averaged information. Mitigate this problem, an autoregressive (AR) modeling method has been proposed for analysis of HRV signals, but this method subject to error from model misspecification (selecting order). However, as the HRV signals have a place with the group of multicomponent non-stationary signals (Wood and Barry, 1996). It is challenge to obtain precise assessments of time-varying spectral signals, due to the sudden cardiac death, precise classification and early detection are necessary for the cardiac diseases subjects. This problem can tackle by an appropriate time–frequency distribution method and resolute the multicomponent behavior of HRV and respiratory signals (Kamath *et al.,* 1996; Dliou *et al.,* 2014). The fundamental target of time–frequency investigation is to create a function that will portray the power density of a signal concurrently in time and frequency without cross-terms, if exist (Dliou *et al.,* 2014). Since the HRV waveform reflecting numerous parts of the physical state and activity of the human heart, it is important for the processing techniques to detect the different basic components of HRV complex without cross term with excellent resolution. As HRV waveform is multicomponent signals and exists cross term. Therefore, the time–frequency techniques are appropriate for analysis of HRV signals (Addison, Walker and Guido, 2009).

Recently, many time-frequency methods such as short time Fourier transform (STFT), Wigner -Ville distribution (WVD), Choi Williams Distribution (CWD), and Born Jordan Distribution (BJD) are available for high-resolution, within the time-frequency plane decomposition. To evaluate ECG arrhythmia, these approaches are useful (Addison, 2005; Boashash, 2015). These strategies are helpful for graphical record heart disease analysis (Addison, 2005; Boashash, 2015). However, these strategies have advantages and drawbacks once victimisation for abnormal knowledge of HRV signal analysis in time-frequency domain (Dliou *et al.,* 2014). Over the past few years, the wavelet transforms (WT) has evolved in the time frequency domain to analyze and code HRV and respiratory signals. WT is a computational tool that allows us to decompose a multicomponent of HRV into a representation that shows approximation of signals and sub-sets as time variable. This illustration utilizes to characterize transient events (a signal contains incoherence), compress knowledge, and reduce noise, sharp peak detection. and features extraction from HRV complex signal which are useful for precise diagnosis of cardiac diseases. As we have found in this survey, the WT has ability to isolate out apropos signal from multicomponent signal, has prompted various wavelet-based procedures which supersede those in view of conventional Fourier strategies. In this literature survey, we have seen that WT has been utilized as either in the form of continuous or discrete with appropriate classifier for detection and classification of arrhythmias subjects. The WT in continuous form, that is known as CWT, permits an intense investigation of arrhythmias in HRV signal, making it in a perfect global suited for the high-determination cross examination of the HRV signals over an extensive variety of uses. The WT in discrete form, i.e. known as Discrete wavelet transform (DWT), provide the basis of powerful approaches for filtering, partitioning pertinent signal components which help as a source for potent pattern recognition strategies arrhythmias HRV signals. The CWT method allows for discretionarily high resolution of HRV signals within the time-frequency plane distribution, that could be a would like for the correct segregation of acceptable segments and distinctive of arrhythmias HRV signals. However, the DWT applying for analysis for HRV signals, it leads problems in terms of robustness and repeatability of the analysis, if it is not built-in ensemble averaged method. The performance of DWT can be improved by implementing it with digital signal processing (DSP) tool (Gutiérrez-Gnecchi *et al.,* 2017).

2. METHODOLOGY

2.1 ADAPTIVE CONTINUES MORLET WAVELET TRANSFORM

2.1.1 CONTINUES MORLET WAVELET TRANSFORM

The Continues Morlet Wavelet Transform (CMWT) of a time series signal X_t is definite as

$$W_t\,(s,a)= \langle s,\Phi_{s,a}\rangle=\frac{1}{\sqrt{s}}\int_{\infty}^{+\infty} X_t\,\Phi^*\left(\frac{t-a}{s}\right) dt \tag{1}$$

Here $\Phi^*(t)$ is that the complex conjugate of the mother wavelet $\Phi(t)$, is that the real positive range, denotes the scaling parameter of the mother wavelet and *a is* also a real number, that dilates the scaled the scaled mother wavelet with time axis (Mallat, 1989). The Morlet wavelet comprises a plane wave modulated by Gaussian (Daubechies, 1992), the Morlet wavelet operate is drawn in time domain as

$$\Phi_M(t)=\pi^{-\frac{1}{4}}\left[e^{-iwot}- e^{\frac{-w\delta}{2}}\right] e^{\frac{-t^2}{2}} \tag{2}$$

Its FT is defined in equation in (3), shifted Gaussian function and satisfies the admissibility condition so that

$$\widehat{\Phi}_M(w)= \pi^{-\frac{1}{4}}\left[e^{-\frac{(w-w_0)^2}{2}} - e^{\frac{-w\delta+w^2}{2}}\right] \tag{3}$$

Here is the central frequency of the Morlet wavelet. We have chosen to satisfy the admissible condition in this review paper (Orović *et al.,* 2011) and in practice the second term of equation (2) and (3) can be overlooked. The function of the Morlet wavelet and its Fourier transform becomes

$$\Phi_M(t)= \pi^{-\frac{1}{4}}\, e^{-iw-w_0t}\, e^{-\frac{t^2}{2}} \tag{4}$$

FT of scaled by '*s*' of mother Morlet wavelet function written as

$$\widehat{\Phi}_M(sw)= \pi^{-\frac{1}{4}}\, e^{-\frac{(sw-w_0)^2}{2}} \tag{5}$$

The CMWT improved the energy concentration by adding a shape parameter to the parameter to the Morlet wavelet function Gaussian component, which interacts with time and frequency resolution (Belsak and Flasker, 2010). The shape parameter **may be a perform** of frequency, **therefore** the Morlet **wave perform** of equation (4) becomes as

$$\Phi_M(t,\lambda)= \pi^{-\frac{1}{4}}\, e^{-iwot}\, e^{\frac{\lambda^2t^2}{2}} \tag{6}$$

As γ is function of frequency, hence (f) = 1/f and equation (6) becomes

$$\Phi_M(t,\lambda(f))= \pi^{-\frac{1}{4}}\, e^{-iwot}\, e^{-\frac{t^2}{2f^2}} \tag{7}$$

It's FT with scaled becomes

$$\widehat{\Phi}_M(sw,\ f)= \pi^{-\frac{1}{4}}\, e^{-\frac{f^2(sw-w_0)2}{2}} \tag{8}$$

2.1.1 ADAPTIVE MORLET WAVELET FUNCTION

To make the adaptive of CMWT, a new parameter β is added to the shape parameter. Hence $\lambda(f)=1/f^{\beta}$. The new parameter can control the λ shape parameter of the Morlet wavelet function. The value of β was selected from a set $0<\beta<1$, when $\beta=C$ corresponding to equation (4) of Morlet wavelet function and $\beta=1$ corresponding to the equation (7) of Morlet function. By calculating an optimal value of β i.e. say (β_{opt}), the maximum energy concentration measurement (ECM_{max}) can be obtained. Method to find β_{opt} has been explained in section 2.1.2. Thus, adaptive Morlet function and its FT becomes

$$\Phi_M(t,\lambda(f))= \pi^{-\frac{1}{4}}\ e^{-iw_0 t}\ e^{-\frac{t^2}{2f^{2\beta}}} \tag{9}$$

$$\widehat{\Phi}_M(sw,\ f)= \pi^{-\frac{1}{4}}\ e^{-\frac{f^2(sw-w_0)2}{2}} \tag{10}$$

If adaptive Morlet function set in place of mother wavelet Φ(t), then CMWT is known as ACMWT. The algorithm of global method is shown in **Figure1.**

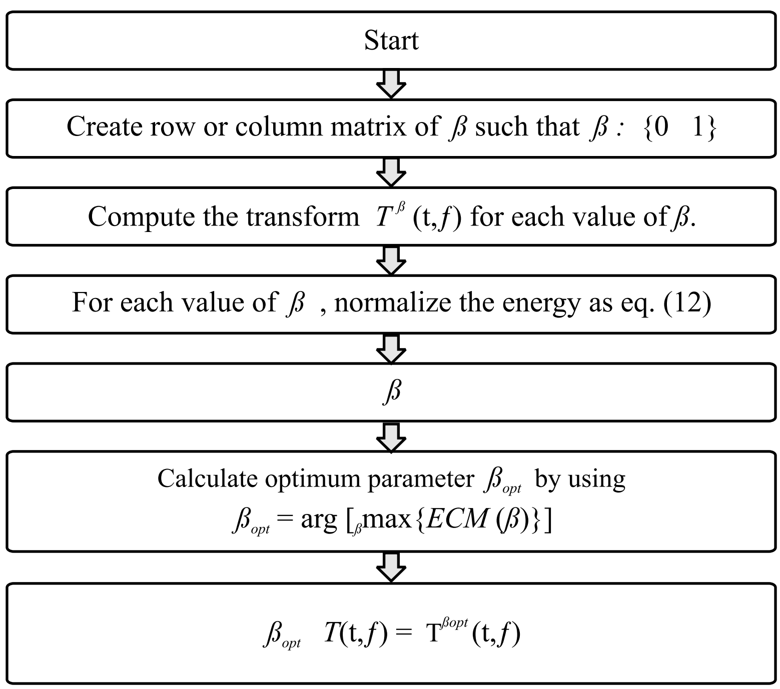

Figure 1: The algorithm of global method

2.1.3 ALGORITHM TO DETERMINE β_{opt}

The calculation of β_{opt} depends on energy concentration measurement (ECM). The β_{opt} value of β can be determined by using a global method, in which value of q invariant for entire signal (Djurović, Sejdić and Jiang, 2008; Stankovic, 1997). . Advantage of this method is to give exceptional temporal and spectral resolution. The ECM is defined as

$$ECM(\beta) = \frac{1}{\iint_{-\infty}^{+\infty} T^{\beta(t,f)} dt df} \tag{11}$$

Symbol $T^{\beta}(t,f)$. is used for any time-frequency transform (like ACMWT) for a value of β. The normalized energy $T^{\beta}(t,f)$ defined as

$$T^{\beta}(t,f) = \frac{T^{\beta(t,f)}}{\sqrt{\iint_{-\infty}^{+\infty} | T^{\beta(t,f)}|^{2\, dt\, df}}} \tag{12}$$

3. STATISTICALANALYSIS

Statistical analysis was performed using t-test for comparison of low frequency power (LFp), high frequency power (HFp) and LFp /HFp ratio values (taken mean of median of interquartile values) between HRV of healthy young group subject and HRV of healthy elderly group subjects. All 'p' values are calculated for one-tailed test at $p<0.05$ was considered statiscally significant. Results are reported as Mean±S.d. The ^{ECMAX} of individual synthetic characteristics of HRV signals was calculated at significance level $^{(\alpha) = 50\%}$ without noise and signal to noise ratio (SNR)= 30 dB for each considered time-frequency transform methods.

4. MATERIALS

2.1.1 SYNTHETIC TEST SIGNALS

In order to validate the time frequency transform (TFT) methods which are described in **Table 1.** Four synthetic signals are generated, which are sampled at 4Hz and duration of $0 \leqslant t \leqslant 300$ S. The synthetic signals are listed in **Table 2**. The characteristics (stationary and non-stationary) of synthetic signals were modeled as individual physiognomies of HRV signals. The instantaneous frequency of each component of synthetic signals is determined by $f(t) = d\Phi/2\pi\, dt$, here Φ is angle of each cosine component of synthetic signals. The stationary characteristics of synthetic signal related to Mayer- wave (around 0.1Hz in LF band) and respiratory sinus arrhythmia (RSA) (around 0.4 Hz in infant or 0.25 in HF band). All the possible non-stationary characteristics like, all possible frequency range of sympathetic and parasympathetic activity (i.e. increased or decreased the heart rate) and respiratory frequencies observed in many autonomic tests has been covered in the used non-stationary generated by the dynamical model in this study(Mc Sharry *et al*., 2003) (Orini *et al*., 2012). The change in heart rate depend on influence like person's activity level, posture, recent diet, degree of fitness, age and health (Siegel *et al*., 2004). From theoretical view point, the tracking of time varying, slow or fast spectral components of HRV signals characterized by sinusoidal frequency modulation is challenging due to the high level of inner interference among signals with such a modulation. In this situation, separating LFp and HFp components of HRV signals requires high ECM or resolution and applied method to analysis of HRV should follow the ideal time-frequency mapping.

2.1.1 DATABASE

For this study, the database used in the analysis of cardiovascular signals was obtained from the Fantasia Database (Goldberger *et al*., 2000) has the records f2o01, f2o02... f2o10 from the healthy elderly subjects (70– 82 years old) and records f2y01, f2y02... f2y10 from the healthy young subjects (23–32 years old). The subjects underwent two hours. of continuous supine resting whereas uncalibrated continuous non-invasive continuous electrocardiogram and respiration signals were collected. Every cluster contains eight subjects, within which equal range of females and men. All subjects continuing during a resting state in sinus rhythm whereas observance the moving picture Fantasia (Disney, 1940) to assist carries on wakefulness. The continuous blood pressure and ECG signals were digitized at 250Hz (lyengar *el al*.,, 1996; Moody and Mark, 2001). For the self-recoded data, the recording of ECG was done at the sampling rate of 500 Hz with BIOPAC ® MP150 in combination with BIOPAC's "Acqknowledge ® 4.2" software. For short term analysis, we have selected 30 minutes recording of each data, the first 20 minutes and last five samples have been excluded from each group of epoch so that all the subjects were alleviated to the recording atmosphere. This will provide the prospect for group of subject evaluation as under same activity level. The R peaks of the ECG signal were detected using modified Tompkins's algorithm (Greenwald, Patil and Mark, 1992). The R-R interval time series for each subject was then computed.

4.1.3 PRE-PROCESSING OF HRV SIGNAL

Pre-processing of R-R interval time series data is required before analysis of HRV signal to reduced error and enhances the sensitivity of time series data. First we've done ectopic beat or interval detection, correction, and resampling before HRV analysis. In this article, the position beats were detected on the premise of normal deviation filter methodology that marks outliers as being intervals that lie outside the mean IBI by a user outlined price of standard deviation. The user outlined price was used as three times of normal deviation (Pan and Tompkins, 1985). A cube like spline interpolation methodology was accustomed replace position intervals based throughout the HRV and respiratory signal detection method. By exploitation cube like spline methodology the R-R intervals were resampled at four Hz.

5. RESULTS

5.1 SIMULATION STUDY OF SYNTHETIC SIGNALS

Table 1: Time domain and Frequency domain representation of Morlet wavelet function, Stockwell function and their resolution factor along with scale to frequency factor.

Function	Time Domain	Fourier transform	Resolution factor	Scale to freq. factor
Morlet wavelet function	$\pi^{-\frac{1}{4}}\ e^{-iw_o t}\ e^{-\frac{t^2}{2}}$	$\pi^{-\frac{1}{4}} H(w)\ e^{-\frac{(aw-w_o)2}{2}}$ With scale factor 'a'	α	$\frac{4\pi\alpha}{w_0+\sqrt{2+w_0^2}}$
Adaptive Morlet wavelet function	$\pi^{-\frac{1}{4}}\ e^{-iw_o t}\ e^{-\frac{t^2}{2f^{2q}}}$	$\pi^{-\frac{1}{4}} H(w)\ e^{-\frac{f^{2q}(aw-wo)^2}{2}}$ with scaled 'a'	a, f and q	$\frac{4\pi\alpha}{w_0+\sqrt{2+w_0^2}}$
Adaptive ST function	$\frac{\lvert f\rvert^q}{\sqrt{2\pi}} e^{--\frac{f^{2q}t^2}{2}}$	$e^{-\frac{2\pi^2 y^2}{f^{2q}}}$	f and q, When q =1 then ST function.	Not Applicable
Adaptive Modified ST function	$\frac{\lvert f\rvert}{\left(\frac{1}{N} f + q\ var(sign.)\right)\sqrt{2\pi}}$ $\mathrm{x}e^{-\frac{f^2 t^2}{2\left(\frac{2}{N} f + q\ var(sign.)\right)^2}}$	$e^{-\frac{2\pi^2 (\frac{1}{N}f+q^{var\ (sign.)})y^2}{f^2}}$	f and q	Not Applicable
Note: H(w) is a Heaviside step function used for analytical wavelet , {H(w)=1 if w>0 ,H(w)=0 otherwise }				

Table 2: Example of synthetic test signals and their characteristics and Sampling frequency (Fs), duration of signals.

Experiment	Synthetic test signal	Characteristics	(Fs) and duration
1.	$Y_2(t) = \mathrm{Cos}(0.518\pi t + 183\pi \times 10^{-6} t^2)$ $+\mathrm{Cos}(0.0392\pi t - 261\pi \times 10^{-7} t^2)$ $+\mathrm{Cos}(0.118\pi t + 784\pi \times 10^{-7} t^2)$	Non-stationary and slowly time varying spectral components Hz,	*Fs* = 4 Hz, $0 \leqslant t \leqslant 300$ *Sec.*
2.	$Y_4(t) = \mathrm{Cos}(0.078\pi \log(\frac{10t+300}{300}))$ $+\mathrm{Cos}(0.188\pi t + 104 \times 10^{-6} \pi t^2)$	Non-stationary and fast frequency variation signal	*Fs* - 4 Hz, $0 \leqslant t \leqslant 300$ Sec.

Table 3: ECMmax values for different TFT methods under noise free and with AWGN SNR of 30 dB for experiment 1.

TFT estimator	ECMmax Noise free	ECMmax, AWGN with SNR 30 dB
CMWT $w_0 = 6$	0.1324	0.1310
ACMWT $w_0 = 6$ $q_{opt} = 0.31$	0.1761	0.1705
ST	0.1393	0.1369
AST $q_{opt} = 0.11$	0.1746	0.1675
AMST $q_{opt} = 0.25$	0.1753	0.1681

Experiment 1. The second synthetic test signal $y_1(t)$ as in **Figure 1. (a)** is non-stationary signal and slowly time varying spectra components. It consists of three signals having frequency range (0.26-0.31Hz), (0.06–0.08Hz) and (0.018-0.012Hz). The sampling frequency used is 4 Hz and exists in the interval $0 \leqslant t \leqslant 300$s. The power spectra of ACMWT $w_0 = 6$ estimator is shown in **Figure 1.(c).** It show clear picture of all three components of signal, either LF or HF band. It is also observed from simulated data, reported in **Table 3**, it has higher **ECMmax** compared to all considered TF estimator. After the ACMWT at $w_0 = 6$ method, the AMST is depicted in **Figure 1.(f)** has better **ECEmax** (resolution) compared to AST, ST and CMWT at $w_0 = 6$ But AMST, AST and CMWT show poor resolution of frequency component signals in the range of LF band (0.06-0.08 Hz), Which are shown in **Figures 1.(e), (d)** and **Figure 1. (b).** Hence, the ACMWT at $w_0 = 6$ is more appropriate technique, where power spectra of HRV signals varies slowly with time. When AWGN noise of 30 dB introduced with signal $y_2(t)$, reported in **Table 3,** the of **ECMmax** CMWT decreased from 0.1324 to 0.1310, ACMWT decreased from 0.1761 to 0.1705, AST decreased from 0.1746 to 0.1675 and AMST decreased from 0.1753 to 0.1681 in noisy environment, but ACMWT at $w_0 = 6$ estimator at $q_{opt} = 0.31$ still performs better.

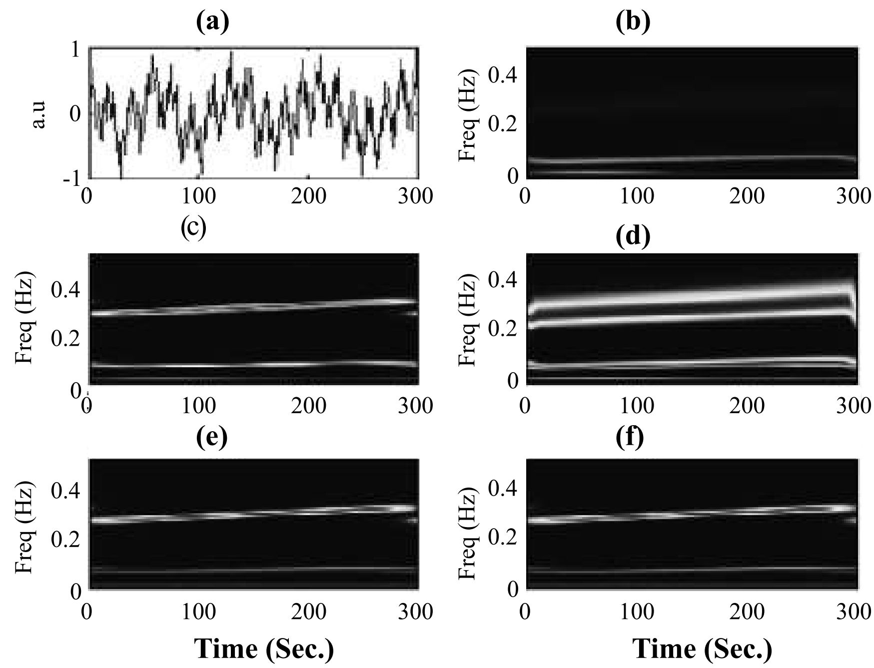

Figure 1: Time–Frequency power spectra maps of signal (a) time-domain representation of test signal $Y_2(t)$ having arbitrary unit (a.u) amplitude, assessed by (b) CMWT at $w_0 = 6$ (c) ACMWT at $w_0 = 6$ (d) ST (e) AST and (f) AMST

Table 4: ECMmax values for different TFT methods under noise free and with AWGN SNR of 30 dB for experiment 2.

TFT estimator	ECMmax Noise free	ECMmax, AWGN with SNR 30 dB
CMWT $w_0 = 6$	0.1757	0.1717
ACMWT $w_0 = 6$ $q_{opt} = 0.21$	0.1916	0.1846
ST	0.1736	0.1661
AST $q_{opt} = 0.30$	0.1898	0.1790
AMST $q_{opt} = 0.15$	0.1895	0.1789

Experiment 2. The last synthetic signal $y_4(t)$ is depicted in **Figure 2.(a)** is one of the important classes of non-stationary signal, in which there exist crossing components that content with fast frequency variation. The $y_4(t)$ signal is mixture of two signals, one rapidly transit from lower to higher frequency region (0.04 – 0.4Hz) and the other linearly varies frequency (0.1 – 0.12Hz) with time as chirp signal. This signal was sampled at 4Hz and exists for the duration $0 \leq t \leq 300$s. The power spectra of signal $y_4(t)$ was assessed by ACMWT at $w_0 = 6$ at $q_{opt} = 0.21$ is shown in **Figure 2.(c)**. The temporal and spectral resolution is excellent up to the crossing component of fast varying frequency component and linear chirp signal. While the resolution after the crossing components of fast varying frequency slightly fade. In spite of this, as the data statement reported in **Table 2**, the ACMWT at $w_0 = 6$ method has better **ECMmax** compared to other considered method. The AST for $q_{opt} = 0.30$ is shown in **Figure 2.(e)** and AMST for $q_{opt} = 0.15$ is shown in **Figure 2.(f)** has better resolution than ST, as in **Figure 2.(d)** and CMWT as in

Figure 2. (b). On the basis of simulated data reported in **Table 4**, these methods have also **ECMmax** high compared to the ST and CMWT. Hence, the ACMWT at $w_0 = 6$ is best estimator, where power spectra of HRV signals is fast varying with time. Above 0.16 Hz frequency (crossing point), CMWT and ACMWT show poor resolution which are depicted in Figure 2.(b) and Figure 2.(c).

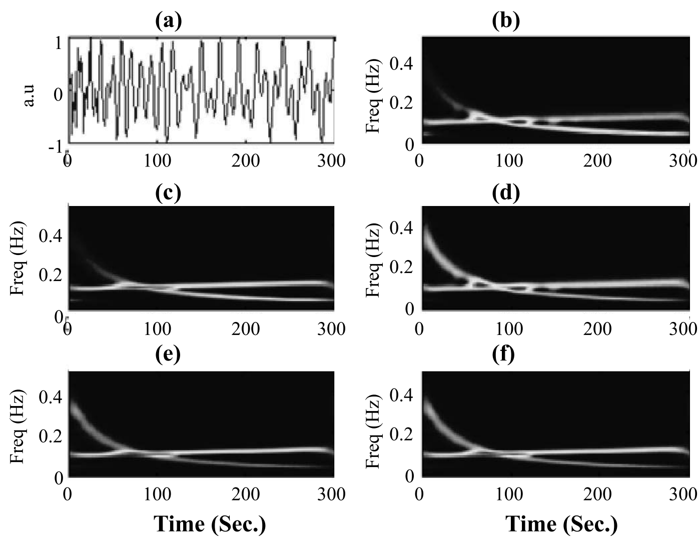

Figure 2: Time-Frequency power spectra maps of signal (a) time-domain representation of test signal $Y_4(t)$ having arbitrary unit (a.u) amplitude, assessed by (b) CMWT at $w_0 = 6$ (c) ACMWT at $w_0 = 6$ (d) ST (e) AST and (f) AMST

5.2 MODEL GOODNESS-OF-FIT

Assume in a given observation interval {O,*T*}, K successive HRV wave events were recorded as $O<C_1<C_2<...<C_k<T$. Given any HRV wave event C_k, the waiting time ($\vartheta(t)$ until the subsequent HRV wave event follow the history dependent inverse Gaussian Probability Density . In order to estimate how well the proposed method ACMWT describes a time series HRV signals, it is required to compute goodness-of-fit (GOF) statistics. The GOF technique is calculable exploitation Kolmogorov-Smirnov (KS) take a look at designed on the time-rescaling formula (Brown *el al.*, 2002) . The KS test uses the intensity function is defined as Eq. (13)

$$\rho(t) = \frac{\vartheta\,(t)}{[1-\int_{C_n}^{t}\vartheta(u)du]} \tag{13}$$

Then, time scaled or transformed HRV can be defined as Eq. (14)

$$t_n = \int_{C_{n-1}}^{C_n}\vartheta(t)dt \tag{14}$$

Where t_n values are independent exponential random variables with a unit rate. It is transformed into $Z_k=1-e^{(-tk)}$ which are uniform independent random variables on the interval {0, 1}. The KS strategy (Ogata, 1988) allows to validate the arrangement between the Z_k and the ideal uniform probability density function. If the method is accurate, the KS plots should line up with the 45 degrees diagonal. Furthermore, KS distance can be calculated as the maximum distance between the cumulative distribution function (CDF) of Z_k and the CDF of ideal uniform distribution on {0, 1}. Besides, the KS strategy, autocorrelation function (AFC) within the variety of remodelled quantiles is computed **to see** the independence of the transformed intervals (Barbieri, 2004). AFC for given HRV signals as $H_1,H_2,..........H_n$ at time $t_1,t_2,..........t_n$ for the lag (*K*)autocorrelation function (*AFC*) is defined as Eq. (15)

$$AFC = \frac{\sum_{i=1}^{n-K} (H_i - \mu)(H_{i+K} - \mu)}{\sum_{i=1}^{n-K} (H_i - \mu)^2} \tag{15}$$

Where μ denotes the mean value of HRV signals in transformed intervals t_n. As indicated by the time-rescaling hypothesis (Brown *el al.*, 2002), t_n values must be independent irrespective of the dependencies in the HRV time series. We plot the AFC of the t_n values at different value of *K*, with the aim of assess the correlation structure. If AFC has small values of the at all *K* would suggest that the t_n values are uncorrelated, so reliable with independence conditions (Baarbieri, 2004). It is indicating that the proposed method is appropriate for the HRV time series.

5.2.1 SIMULATION STUDY OF SYNTHETIC RESPIRATORY AND HEART RATE VARIABILITY SIGNAL

The ACMWT method is tested with synthetic signals like constant and variable respiratory conditions in order to estimate the robustness of this proposed method. A simple sinusoidal model having characteristics of both HRV and respiratory (REP) signals is defined by Eq. (16) and Eq. (17)

$$HRV(t) = SD_{HRV} + \delta(t)\,sin(2\pi\, F_1(t)t) + \sigma(t)\,sin\,(2\pi F_2(t)t) + N_2(t) \tag{16}$$

$$REP(t) = \alpha(t)\,sin(2\pi\, F_2(t)t) + N_1(t) \tag{17}$$

Where F_1(t) and F_2(t) with strength factors δ(t) and σ(t) are the LF and HF frequency components of the synthetic *HRV*(*t*) and SD_{HRV} is standard deviation of HRV signal. In this modeled the HF frequency component of HRV signal is correlated with the REP signal by including frequency $F_2(t)$ in the REP signal. The strength of the REP waveform is sculpted by α(t). $N_1(t)$ and $N_2(t)$ are noise in the HRV signal and REP signal are inserted by AWGN. The characteristics of these signals was modeled as dynamic autonomic inputs via setting the δ(t) and σ(t) parameters, therefore changing the LF_p and HFp. The LFp/HFp ratio, which is given by {δ(t)/σ(t)}, can subsequently also be varied. The model is additionally capable of varied the respiratory sinus arrhythmia (RSA) gain by dynamical the ratio of σ(t)/α(t) magnitude relation. The proposed methodology is employed to perform two artificial sets of simulations for estimation of the dynamic RSA gain at constant and dynamic respiration conditions by dynamical the worth of solely and ranging each and , individually. These two sets of simulations are reported in **Table 5**.

Table 5: Parameters used in simulation of RSA for constant REP and varying REP frequency. REPU indicates respiratory unit.

Sets	SD_{HRV}	$F_1(t)$	$F_2(t)$	$\delta(t)$	$\sigma(t)$	$\alpha(t)$
1.Constant REP Frequency	1.5 s	0.15HZ	0.25 Hz	0.1s	0.24, 0⩽t<100s 0.15, 100⩽t<200s 0.15-0.24 s, 200⩽t⩽300s	0.12 REPU
2.Time Varying REP Frequency	2 s	0.15 Hz	0.18-0.3Hz, 0⩽t<100s 0.3Hz, 100⩽t<200s 0.18 Hz, 200⩽t⩽300s	0.1s	0.24, 0⩽t<100s 0.15, 100⩽t<200s 0.15-0.24 s, 200⩽t⩽300s	0.12 EPU

5.2.2 *CONSTANT RESPIRATORY FREQUENCY*

The proposed method is tested on first set of simulations, listed in **Table 5**. The simulation depicts that proposed method is capable of precisely assessing the RSA gain while REP frequency remnants relatively constant and the results are demonstrated in **Figure 3.(b).** The parameter $\sigma(t)$ is kept to have a rapidly change from 0.24s to 0.15s at 100s, and then a linearly varying from 0.15s to 0.24s between 200s and 300s in order to validate the capability of the proposed method to track step variation along with gradual variation in RSA gain however REP frequency remains constant is shown in **Figure 3 .(b)** AWGN is used for $N_1(t)$ and $N_2(t)$ with SNR set at 30 dB. The step variation at 100s is traced accurately, and the proposed method is capable of getting 95% of the lower RSA level within 40s. Besides, gradual variations in RSA from 200s to 300s are also tracked accurately. The KS plot between quintiles and empirical quintiles, and autocorrelation function (AFC) for 50 lags in the form of the transformed quintiles' are depicted in **Figure 4.** The KS plot is shown in **Figure 4.(a)** depicts that the graph line up with the 45 degrees diagonal and AFC for most lags stays well within the 95% confidence interval is shown in **Figure 4.(b).** Hence, proposed method show GOF statistics for synthetic HRV signal.

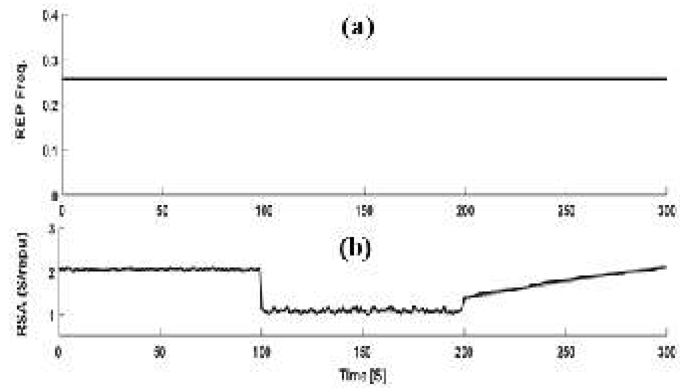

Figure 3: Represents (a) frequency of constant REP synthetic signal (b) RSA gain of the synthetic HRV at constant REP frequency. Dotted red line indications the theoretically RSA gain.

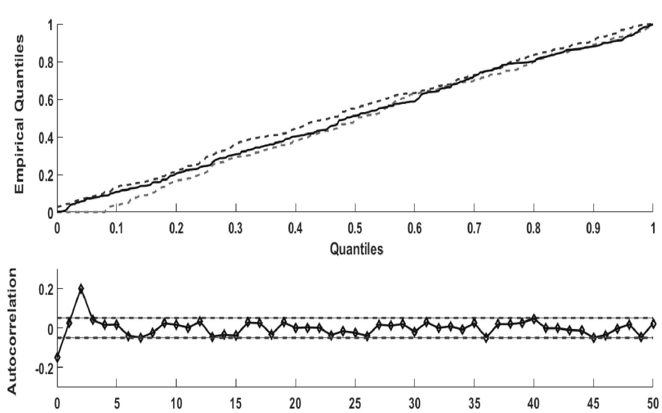

Figure 4: Represents for constant frequency (a) KS plot (b) AFC in the form of transformed quantiles' demonstrate the, dashed red lines indicate the 95% confidence interval.

5.2.3 *VARYING RESPIRATORY FREQUENCY*

The proposed method is validated on second set of synthetic signals. The simulation depicts that proposed method is still capable of accurately assessing the RSA gain however REP frequency slowly and abrupt changes in the REP frequency, and the results are demonstrated in **Figure 5**. In this case, REP frequency F_2(t) is linearly increased from 0.18Hz to 0.3Hz between 0s to 100s, constant frequency as 0.3Hz between 100s to 200s and rapidly returning back to 0.18 Hz at 200s, is shown in **Figure 5. (a).** All the remaining parameters are set at same as 1st set.

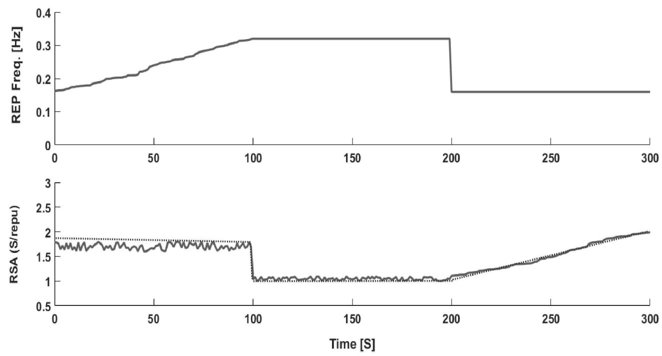

Figure 5 : Represents (a) frequency of variable REP synthetic signal (b) RSA gain of the synthetic HRV at variable REP frequency. Dotted red line indications the theoretically anticipated RSA gain.

The assessed RSA gain fluctuates below approximately 2 during interval (from 0s to 100s) when the REP frequency slowly increases from 0.18Hz to 0.3Hz. This shows the robustness of the proposed method under changed REP frequency is shown in **Figure 5 (b)**. The abrupt change in the REP frequency at 100s does not show an influence on precise assessment of RSA gain during period from 100s to 200s. **Figure 6** illustrations the KS plot in **Figure 6.(a)** and the AFC in the form of transformed quantiles in **Figure 6.(b)**, which validate the GOF of the proposed method. The simulation results show that the proposed method is proficient of assessing the RSA gain exactly under variation of respiration patterns and autonomic inputs. The approach properly tracks fast fluctuations in RSA, therefore providing accurate instantaneous RSA assessments.

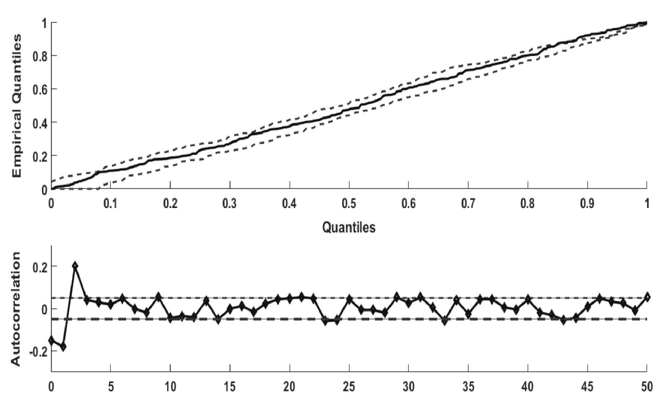

Figure 6: Represents for variable frequency (a) KS plot (b) AFC in the form of transformed quantiles. Dashed red lines indicate the 95% confidence interval.

5.2.4 TIME-FREQUENCY ANALYSIS OF REAL HRV AND REP SIGNAL

After validating the proposed method on synthetic signals, T-F analysis of HRV, REP, and RSA gain due to REP is done for each subject with the aim of recognize the dynamic REP frequency and the dynamic frequency where maximum gain take place, as a preliminary step for evaluating dynamic RSA. The wave form of physiological signals like HRV and respiratory of a young subject in time domain is shown in **Figure 7. (a)** and **Figure 7. (b),** and their power spectral in time-frequency domain is shown in **Figure 8. (b)** and **Figure 8.(d).** The proposed method ACMWT is used for analysis of HRV and REP signals in T-F domain. T-F plots of HRV and REP signals are presented in **Figure 8** for the elderly and young subject. From the T-F distributions of REP and RSA gain, it is manifest that frequency of maximum RSA gain closely matches with the REP frequency. It indicates that the highest correlation between HRV and REP commonly take place at the predominant REP frequency. In Young subject, a notable drop in the predominant REP frequency (both inspiration and expiration) is observed during 100 to 280s around 0.25Hz, which is shown in **Figure 8.(d)**. However REP frequency drops to around 0.18Hz in the elderly subject, which is shown in **Figure 8.(c).** As elderly subjects exhibit altered in respiration, it is likely due to sustain a deep breathing. Therefore, a consistent approach for ANS control assessment should be able to elucidation for a different range of REP dynamic vicissitudes. As the proposed method relies on estimates of instantaneous respiratory frequency to compute the RSA gain, it is possible to follow such variations in breathing. In young subject considerable increase in RSA gain is evidently noticeable and having high energy concentration. While in the elderly subject RSA gain appears to spread across approximately entire T-F map and having light energy concentration. It may be due to degradation of ANS with aging.

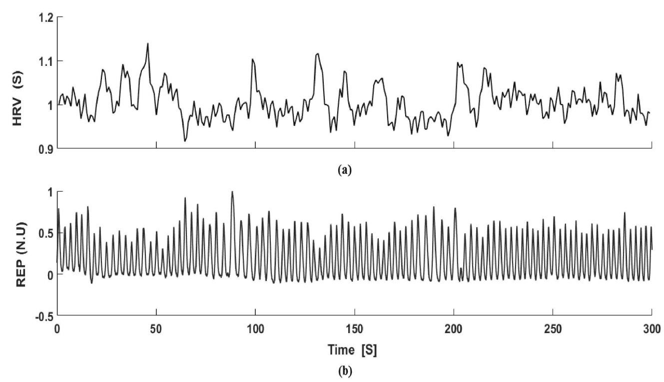

Figure 7: Time domain representation of (a) HRV signal after pre-processing (b) Respiratory signal of healthy young subject, N.U. indicates normalized unit.

The GOF model is again validated against the standard Fantansia database using KS plots and AFC in the form of transformed quantiles for Young is shown in **Figure 9. (a-b)** and Elderly subjects, as shown in **Figure 9. (c-d).** For this analysis, HRV data of 21 young and 16 elderly subjects are used. The KS plots nearly follow the CDF of the uniform distribution and mostly around the 95% confidence interval for Young subjects is shown in **Figure 9.(a).** While this plot is approximately line up with the 45 degrees diagonal **for** Elderly subjects is illustrated in **Figure 9.(c).** These small variations in KS distance further show that the model also fits well for the standard database. Furthermore, AFC in the form

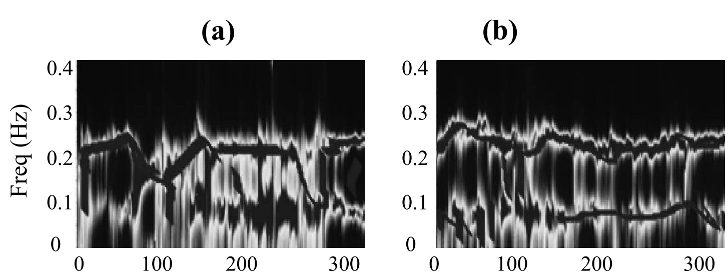

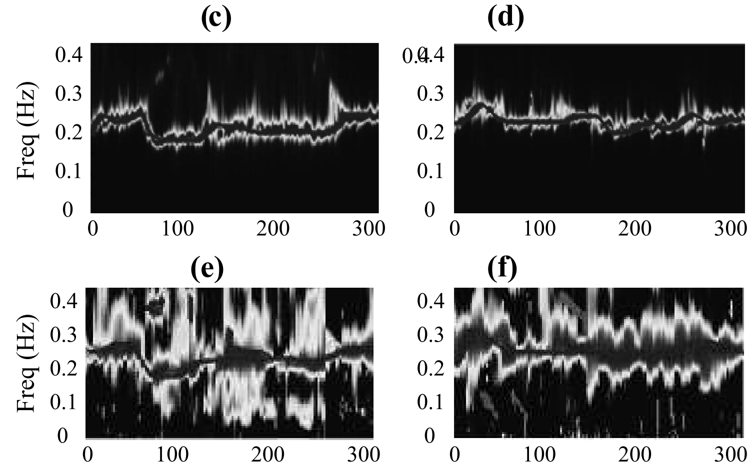

Figure 8: Represents Time-frequency (a) power distributions of HRV of an Elderly subject (b) power distributions of HRV of a Young subject (c) power distributions of REP of an Elderly subject (d) power distributions of REP of a Young subject (e) RSA gain of an Elderly subject (f) RSA gain of a Young subject

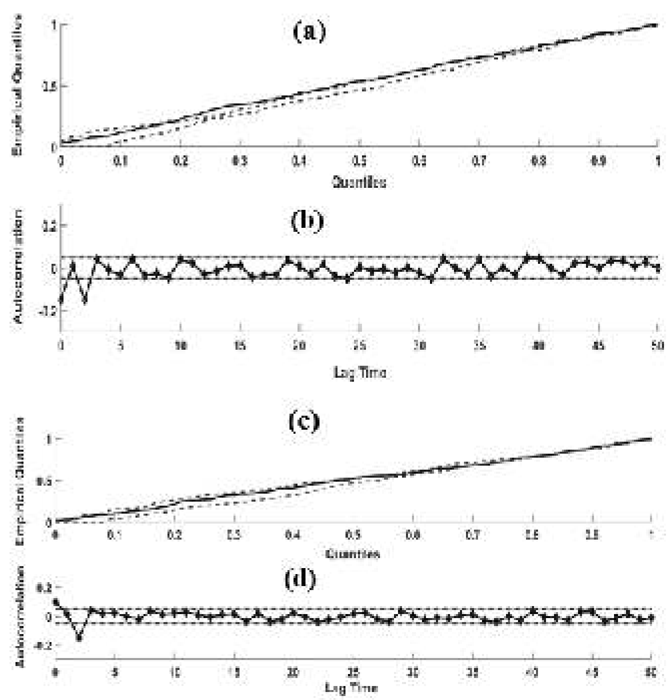

Figure 9: Represents (a) KS plots for Young subject (b) AFC in the form of transformed quintiles' for Young subject (c) KS plots for Elderly subject (d) AFC in the form of transformed quintiles' for Elderly subject. Dashed red lines indicate the 95% confidence interval.

of transformed quantiles plots are also simulated for up to 50 lags (about 60s), and perceived low autocorrelation for elderly and young subjects. The simulated results demonstrates that maximum numbers of AFC points stay within the 95% confidence interval for Young and Elderly subjects both are shown in **Figure 9.(b)** and **Figure 9.(d)**, which implies that the proposed method is also effective for real database.

5.2.5 GLOBAL RESULTS

The results reported in **Table 6** and **Table 7** indicates that the mean value of of power content in HRV of Young male self-recorded (Y_{ms}) are approximately same as HRV of standard Young Fantasia data base (Y_{fan}). However there is a little difference in the mean of LFp/HFp ratio (p= **0.03638)**. This is due to the ECG recorded at different sampling rates, one at 500 Hz and other at 250 Hz. The mean power of HRV of elderly Fantansia (E_{fan}) in VLF, LF and HF are decreased as compared to the mean power of HRV of Y_{ms} and Y_{fan}, while the mean power of HRV of E_{fan} in LF is increased and the HF power is decreased. The autonomic as vagal tone and the sympatho-vagal balance (LFp/HFp ratio) is sympathetic tone dominated . This may be due to the increase of the heart rate or degradation of the autonomic nervous system in elderly subjects. The mean value of LFp/HFp ratio (p=0.00044) of E_{fan} is increased due to increasing in power of low frequency.

Table 6: Mean±SD of power of frequency band of HRV signals for different age group of subjects

No. of subjects	Mean ±SD power (msec2) of VLF	Mean±SD power (msec2) of LF	Mean±SD power (msec2) of HF	Mean±SD of LF/HF ratio
10 Yms (Age 21-32)	15920.7917 ±11528.823	16185.5209 ±5468.545	22802.6789 ±9373.7990	0.7248±0.385
11 Yfan (5M +6F Age 21 -32)	16438.1101 ±15023.42	16988.883 ±14506.89	23083.2648 ±15548.8	0.7802±0.275
16 Efan (9-M+7F Age 70-82)	8558.3980 ±11879.716	2929.8849 ±2512.7342	1505.8700 ±1361.2077	2.9018±2.051

Table 7: P-value using student's T-test (one tailed and unequal variance) of LFp/HFp ratio and VLF power for subjects group Yms = younger male self recorded, Y_{fan} = younger fantasia, E_{fan} = Elderly fantasia.

	Y_{ms}-Y_{fan}	Y_{ms}-E_{fan}	Y_{ms}-E_{fan}
LF/HF p-value	0.03638	0.00145	0.00044
VLF power p-value	0.12984	0.40723	0.08138

6. DISCUSSIONS

To extract meaningful information as LFp and HFp from HRV signals in time-frequency domain is important for experimental science (Rajendra Acharya *el at*., 2013). To obtain correct time-varying spectral density required high resolution without any adjacent interference. There are various signal processing tools to measure important information from HRV signals in time-frequency domain but for correct analysis the results should be analyzed properly (FAUST and BAIRY, 2012). To test the performance (like follow the ideal time-frequency mapping without cross interference, temporal and spectral resolution based on energy concentration) of the adaptive methods was examined using set of synthetic individual characteristics of HRV signals.

In the first experiment for stationary signal, the depiction obtained by the CMWT at $w_0 = 6$ contains large cross terms and poor resolution at HF. The ST suffers from the same problem as the CMWT at $w_0 = 6$ poor resolution at HF and at LF it has good frequency resolution. The AST and AMST methods has more frequency resolution at HF compared to ST and CMWT at , but it not follow the ideal time-frequency mapping. This was evident from Figure 2.3.c, the ACMWT at $w_0 = 6$ has more uniform resolution and follows the ideal time-frequency mapping at both LF and HF. Therefore, the ACMWT certainly enhances the time-frequency (T-F) illustration compared to other considered TFT estimator, and resulting in better energy concentrated time-frequency representation of stationary signals.

By examining the time-frequency representations of the non-stationary signals like slow and fast time varying spectra components, it can be noticed that the ST and CMWT at $w_0 = 6$ are capable to internment the LF components but the energy concentration is poor. The illustration was obtained by AST and AMST contains very good resolution for two components same as ACMWT at $w_0 = 6$, but frequency component signals (0.06- 0.08 Hz, in range of LF band) resolution deteriorate. With the ACMWT the more resolution and better energy concentrated time-frequency representation was obtained for all components of LF and HF compared to other considered T-F methods.

To test the performance, how the adaptive methods behaves for a multi components signals with the crossing components. The time-frequency representation obtained by the ACMWT at $w_0 = 6$, depict that spectral components are well energy concentrated up to the crossing of fast varying frequency component and linear chirp signal and diminishes the cross interference. The ST, AST and AMST have good frequency resolution at HF, but, as the frequency (LF) decreases, the temporal and spectral resolution fades. It also surrounds significant cross interference. Hence, the above discussion shows that the ACMWT at $w_0 = 6$ is capable of enhancing the energy concentration of stationary and non-stationary signals in VLF, LF and HF band of HRV signals and appropriate for the classification of non-stationary signals for example those met in the physiological extents.

7. FUTURE SCOPE

Studies from literature review revealed that precise detection and classification of cardiac arrhythmias is challenge in diagnosing of cardiac diseases by using features extracted from QRS complex of ECG. Albeit numerous researchers, past decade have proposed different strategies to improve them, but still there are necessities for development and modifications. With spectral and WT model, special features like ventricular triggering, *beginning* of *ventricular and* right *ventricular* of volumetric contraction time can be further added to the current features. As features provides always a new indicative patterns. The WT or adaptive WT with classifier can adapt itself by adding new features, and will provide high accuracy with special features considering. The classification accuracy, sensitivity and rate of detection can be improved by adding classifier like extreme learning machine, deep neural networks and probabilistic neural networks with WT and adaptive WT.

8. CONCLUSION

It has been shown that the ACMWT methods in time-frequency domain are a flexible decomposition tool for analysis of multicomponent non-stationary signal which can be used for spectral analysis of HRV and respiratory signals. It is anticipated that the future will see advance utilization of the spectral and wavelet transform to the HRV and respiratory as the developing technologies in view of them are groomed for practical purpose. The results obtained from our proposed method has been depicted that the LFp and HFp power of HRV is decreased in healthy elderly group compared to healthy young subjects, it may be due to degrade in ANS with aging.

9. REFERENCES

Addison, P. S. 2005. 'Wavelet transforms and the ECG: A review', Physiological Measurement.

Addison, P. S., Walker, J. and Guido, R. C. 2009. 'Time--frequency analysis of biosignals', IEEE

Engineering in Medicine and Biology Magazine, 28(5), pp. 14–29.

Barbieri, R. 2004. 'A point-process model of human heartbeat intervals: new definitions of heart rate and heart rate variability', AJP: Heart and Circulatory Physiology, 288(1), pp. H424–H435.

Belsak, A. and Flasker, J. 2010. 'Adaptive wavelet transform method to identify cracks in gears', Eurasip Journal on Advances in Signal Processing, 2010.

Bigan, C. and Woolfson, W. S. 2000. 'Time–frequency analysis of short segments of biomedical data', in IEE Proceedings - Science, Measurement and Technology. IEE, pp. 68–373.

Boashash, B. 1988. 'Note on the Use of the Wigner Distribution for Time-Frequency Signal Analysis', IEEE Transactions on Acoustics, Speech, and Signal Processing, 36(9), pp. 1518–1521.

Boashash, B. 2015. Time-Frequency Signal Analysis and Processing: A Comprehensive Reference, Time-Frequency Signal Analysis and Processing: A Comprehensive Reference.

Brown, E. et al. 2002. 'The time-rescaling theorem and its application to neural spike train data analysis', Neural Computation, 14(2), pp. 325–346.

CJ, M. et al. 2001. 'Diurnal variations of the dominant cycle length of chronic atrial fibrillation', Am J Physiol Heart Circ Physiol, 280(1), pp. H401-6.

Clayton, R. H. and Murray, A. 1993. 'Estimation of the ECG signal spectrum during ventricular fibrillation using the fast Fourier transform and maximum entropy methods', in Computers in Cardiology. IEEE, pp. 2–10.

D. L. Eckberg 1985. 'Human Respiratory-Cardiovascular Interactions in Health and Disease', in Cardiorespiratory and Motor Coordination, pp. 253–258.

Daubechies, I. 1992. Ten Lectures on Wavelets (CBMS-NSF Regional Conference Series in Applied Mathematics), Society for Industrial and Applied Mathematics.

Deng, L. and Yu, D. 2013. 'Deep Learning: Methods and Applications', Foundations and Trends® in Signal Processing, 7(3–4), pp. 197--387.

Djurović, I., Sejdić, E. and Jiang, J. 2008. 'Frequency-based window width optimization for S-transform', AEU - International Journal of Electronics and Communications, 62(4), pp. 245–250.

Dliou, A. et al. 2014. 'Abnormal ECG Signals Analysis Using Non-Parametric Time-Frequency Techniques', Arabian Journal for Science and Engineering, 39(2), pp. 913–921.

FAUST, O. and BAIRY, M. G. 2012. 'Nonlinear Analysis Of Physiological Signals: A Review', Journal of Mechanics in Medicine and Biology, 12(04), p. 1240015.

Goldberger, A. L. et al. 2000. 'PhysioBank, PhysioToolkit, and PhysioNet : Components of a New Research Resource for Complex Physiologic Signals', Circulation, 101(23), pp. e215–e220. Greenwald, S. D., Patil, R. S. and Mark, R. G. (1992) 'Improved detection and classification of arrhythmias in noise-corrupted electrocardiograms using contextual information within an expert system', Biomedical Instrumentation and Technology, 26(2), pp. 124–132.

Gutiérrez-Gnecchi, J. A. et al. 2017. 'DSP-based arrhythmia classification using wavelet transform and probabilistic neural network', Biomedical Signal Processing and Control, 32, pp. 44–56. doi: 10.1016/j.bspc.2016.10.005.

Iyengar, N. et al. 1996. 'Age-related alterations in the fractal scaling of cardiac interbeat interval dynamics.', The American journal of physiology, 271(4 Pt 2), pp. R1078-84.
Kamath, M. V. et al. 1987. 'Heart rate variability power spectrogram as a potential noninvasive signature of cardiac regulatory system response, mechanisms, and disorders', Heart and Vessels, 3(1), pp. 33–41.

Kamath, M. V et al. 1996. 'Detection of Silent Myocardial Ischemia During Ambulatory Monitoring by Time-Frequency Power Spectral Analysis', Annals of Noninvasive Electrocardiology, 1(1), pp. 63–69.

Kamath, M. V and Fallen, E. L. 1993. 'Power spectral analysis of heart rate variability: a noninvasive signature of cardiac autonomic function.', Critical reviews in biomedical engineering, 21(3), pp. 245–311.

Kodituwakku, S. V. W. 2012. Time-Frequency and Point Process Algorithms for Cardiac Arrhythmia Analysis and Cardiorespiratory Control. Australian National University.

Koh, J. et al. 1994. 'Human autonomic rhythms: vagal cardiac mechanisms in tetraplegic subjects.', The Journal of Physiology, 474(3), pp. 483–495.

Mallat, S. G. 1989. 'A Theory for Multiresolution Signal Decomposition: The Wavelet Representation', IEEE Transactions on Pattern Analysis and Machine Intelligence, 11(7), pp. 674–693.

McSharry, P. E. et al. 2003. 'A dynamical model for generating synthetic electrocardiogram signals', IEEE Transactions on Biomedical Engineering, 50(3), pp. 289–294.

Moody, G. B. and Mark, R. G. 2001. 'The impact of the MIT-BIH arrhythmia database', IEEE Engineering in Medicine and Biology Magazine, pp. 45–50.

Ogata, Y. 1988. 'Statistical models for earthquake occurrences and residual analysis for point processes', Journal of the American Statistical Association, 83(401), pp. 9–27.

Orini, M. et al. 2012. 'Characterization of dynamic interactions between cardiovascular signals by time-frequency coherence', IEEE Transactions on Biomedical Engineering, 59(3), pp. 663–673.

Orović, I. et al. 2011. 'A virtual instrument for time-frequency analysis of signals with highly nonstationary instantaneous frequency', IEEE Transactions on Instrumentation and Measurement, 60(3), pp. 791–803.

Pan, J. and Tompkins, W. J. 1985. 'A Real-Time QRS Detection Algorithm', IEEE Transactions on Biomedical Engineering, BME-32(3), pp. 230–236.

R I KITNE 1980. 'An analysis of the thermoregulatory influences on heart-rate variability', The Study of Heart-Rate Variability, 6(1), pp. 81–106.

Rajendra Acharya, U. et al. 2013. 'Automated identification of normal and diabetes heart rate signals using nonlinear measures', Computers in Biology and Medicine, 43(10), pp. 1523–1529.

Schiecke, K. et al. 2014. 'Time-variant, frequency-selective, linear and nonlinear analysis of heart rate variability in children with temporal lobe epilepsy', IEEE Transactions on Biomedical Engineering, 61(6), pp. 1798–1808.

Siegel, P. B. et al. 2004. 'Nonstationary time series analysis of heart rate variability', Circulation, pp. 1–10.

Stankovic, L. 1997. 'Highly concentrated time-frequency distributions: Pseudo quantum signal representation', IEEE Transactions on Signal Processing, 45(3), pp. 543–551.

Vornanen, M., Ryökkynen, A. and Nurmi, A. 2002. 'Temperature-dependent expression of sarcolemmal K + currents in rainbow trout atrial and ventricular myocytes', American Journal of Physiology - Regulatory, Integrative and Comparative Physiology, 282(4), pp. R1191–R1199.

Wood, J. C. and Barry, D. T. 1996. 'Time-frequency analysis of skeletal muscle and cardiac vibrations', Proceedings of the IEEE, 84(9), pp. 1281–1294.